Available online at www.sciencedirect.com
ScienceDirect
International Journal of Solids and Structures 44 (2007) 5894–5911
INTERNATIONAL JOURNAL OF SOLIDS AND STRUCTURES
www.elsevier.com/locate/ijsolstr

Structural damage models for fibrous biological soft tissues

V. Alastrué, J.F. Rodríguez, B. Calvo, M. Doblaré *

Group of Structural Mechanics and Materials Modeling, Aragón Institute of Engineering Research, University of Zaragoza, María de Luna, 3 E-50018 Zaragoza, Spain

Received 24 November 2006; received in revised form 24 January 2007
Available online 8 February 2007

Abstract

This paper presents a comparison between deterministic and stochastically based three-dimensional finite-strain damage models for fibrous biological soft tissues, accounting for separate contributions on damage for the matrix and the fibers. Both models are compared in terms of their numerical performance and qualitative predictions under different loading conditions. Continuum damage mechanics is used to describe the softening behavior of soft tissues under large deformation, making use of the concept of internal variables which provides a very general description of materials involving irreversible effects. In the stochastic model, statistical aspects related to the distribution of fiber length lead to the strain-driven damage model for the fibrous part. Simulations of a uniaxial test, a hollowed plate under biaxial displacement control, and a 3D simulation of a coronary artery undergoing balloon angioplasty are used to compare the performance of both models. Numerical simulations indicate that both models provide similar predictions of damage.

Keywords: Continuum damage; Anisotropic hyperelastic material; Fibrous material; Soft tissue; Artery mechanics

1. Introduction

Accurate constitutive models of soft biological tissue coupled with appropriate numerical approaches can potentially aid for the study of pathologies (i.e., atherosclerosis, heart dysfunction) as well as for the simulation of surgical interventions or accident trauma. This has promoted extensive research in this area in the last few years (Fung, 1993; Humphrey, 2002; Holzapfel and Ogden, 2006). When modeling the mechanical behavior of soft tissue, particular difficulties arise. Several soft biological tissues are subjected to large deformations with negligible volume changes and show an anisotropic mechanical response due to their internal structure. Uniaxial tensile tests (Fung, 1993) and biaxial inflation test (Holzapfel and Weizsäcker, 1998) conducted in soft tissues show an initial low stiffness toe region part with approximately constant stiffness, a second region of increasing stiffness, and a third region corresponding to progressive failure of the composing fibers. On the other hand, the complex structure and composition of these materials also causes a large variability in the

* Corresponding author.
E-mail addresses: jfrodrig@unizar.es (J.F. Rodríguez), mdoblare@unizar.es (M. Doblaré).

0020-7683/$ - see front matter © 2007 Elsevier Ltd. All rights reserved.
doi:10.1016/j.ijsolstr.2007.02.004

mechanical properties (Sacks, 2000), a characteristic that can lead to wrong estimated values for the parameters in the constitutive equations as pointed out by Chew et al. (1986) and Sacks (2003).

Usually, the description of the constitutive behavior of this type of material relies on the identification of an appropriate strain–energy density function from which stress–strain relations and local elasticity tensors can be derived (Holzapfel, 2000). Even though different strain–energy functions have proved to be successful for particular applications and for describing many of the material properties, their use is limited, in most cases, to the range of physiological loads. In fact, most finite element applications have been limited to analyzing the mechanical response of soft tissue into the toe and linear regions (under normal physiological loads), as, for example, Weiss et al. (1996), Pioletti and Rakotomanana (2000), Peña et al. (2005) for ligaments, Billiar and Sacks (2000) for heart valves, Farquhar et al. (1990) for cartilage, and Alastrué et al. (2006) for the cornea.

On the other hand, the large variability in structure and composition exhibited by biological soft tissue makes it necessary to include, to some extent, this information in the definition of the strain–energy function (SEF). In this regard, Lanir (1983) developed a stochastic structural constitutive model in which the orientation of the fibers was modeled using a statistical distribution, whose parameters were estimated numerically by fitting mechanical tests data. Decraemer et al. (1980) and Wuyts et al. (1995) proposed a constitutive model accounting for the composition of the tissue, and assuming collagen fibers to be corrugated in a wavy pattern, with an initial unfolded length following a probability distribution. In this model each collagen fiber obeyed Hooke's law. The model fitted well inflation tests of normal and atherosclerotic human aorta. Another model which accounts for the composition of the tissue and the waviness of the collagen fibers has been recently proposed by Zulliger et al. (2004). They use a log-logistic probability density function with distribution parameters estimated numerically as in the case of Lanir and Decraemer. More recently, Gasser et al. (2006) proposed a constitutive model where the structural tensor is found from the mean fiber orientation of the tissue, accounting also for fiber dispersion. However, these models only considered the elastic response of the tissue.

Only few models have been proposed for describing the mechanical behavior of soft biological tissue with damage. Non-physiological loads drive soft tissue to damage that arises from two possible mechanisms. One would be tear or plastic deformation of fibers. Tear of fibers is consistent with Hurschler's micromechanical model for ligament behavior that includes fiber failure (Hurschler et al., 1997). Similarly, we found the model of Arnoux et al. (2002) and Schechtman and Bader (2002) for ligaments and tendons, or the work of Hokanson and Yazdami (1997) for damaging arteries. However, structural damage models that consider separated contributions on damage from the matrix and fibers are not common. Gasser and Holzapfel (2002) proposed a rate-independent multisurface elastoplastic constitutive model for soft tissue which introduced inelastic deformation of the collagenous component of the tissue. Balzani et al. (2006) proposed a discontinuous damage model for arteries in which damage of the fibers is treated following classical continuous damage theory. This model is similar to the one proposed by Calvo et al. (2006) in which uncoupled anisotropy damage models with separate contributions for the matrix and the fibers is also proposed. Rodríguez et al. (2006) developed a constitutive model which accounts for different damage processes for matrix and fibers. Damage of the fibrous part is incorporated through the statistical distribution of the deformation at the fully extended length of collagen fiber bundles. This implies that model calibration requires working at two scale levels, so the numerical fit is laborious and the computational cost in finite element simulations is expensive.

In this paper, we present a comparison between the two models proposed by Calvo et al. (2006) and Rodríguez et al. (2006). Both models are summarized and the basic expressions for the finite element implementation are derived. The models are tested on displacement-controlled and load-controlled examples and their performance in terms of qualitative results is carried out. The remaining of the paper is organized as follows. Section 2 gives a brief review on the constitutive equations for anisotropic hyperelastic materials. Section 3 describes damage models for biological soft tissues. Section 4 gives expressions for the decoupled elasticity tensor for both models, and Section 5 shows some numerical examples of the application of both damage models previously described. Numerical simulations correspond to a tensile test and a hollowed plate under displacement control, and the simulation of a balloon angioplasty of a coronary artery (a load control case). Section 6 closes with some concluding remarks.

2. Constitutive modeling of hyperelastic fibrous materials

Fibrous soft tissues such as ligaments, cardiac muscle, arteries, and veins are materials composed primarily of connective tissue proteins, elastin and collagen, and smooth cells. These dense connective tissue consist mainly of fibrous elastic tissue grouped in one or several families, embedded in a highly compliant solid matrix (ground substance) (Fung, 1993). It is the presence of these elastic fibers along preferred directions which give the typical anisotropic behavior to these material, with the solid matrix being responsible for their incompressible response. This section reviews basic concepts in finite deformation continuum mechanics and constitutive behavior of fibrous materials.

Let Ω_0 be a continuum body defined as a set of points in a certain assumed reference configuration. It will be also assumed that there exists a one-to-one mapping $\{\boldsymbol{\chi} : \Omega_0 \to \mathcal{R}^3\}$ continuously differentiable (as well as its inverse $\boldsymbol{\chi}^{-1}$) which puts into correspondence Ω_0 with some region Ω, the deformed configuration, in the Euclidean space. This one-to-one mapping $\boldsymbol{\chi}$ transforms a material point $\mathbf{X} \in \Omega_0$ to a position $\mathbf{x} = \boldsymbol{\chi}(\mathbf{X}) \in \Omega$ in the deformed configuration. The direction of a fiber at a point $\mathbf{X} \in \Omega_0$ is defined by a unit vector field $\mathbf{m}_0(\mathbf{X})$, $|\mathbf{m}_0| = 1$. It is usually assumed that, under deformation, the fiber moves with the material points of the continuum body. Therefore, the stretch λ of the fiber defined as the ratio between its lengths at the deformed and reference configurations can be expressed as (see, e.g., Holzapfel, 2000)

$$\lambda \mathbf{m}(\mathbf{x}, t) = \mathbf{F}(\mathbf{X}, t) \cdot \mathbf{m}_0(\mathbf{X}), \tag{1}$$

where $\mathbf{m}$ is the unit vector of the fiber in the deformed configuration with

$$\lambda^2 = \mathbf{m}_0 \cdot \mathbf{F}^T \mathbf{F} \cdot \mathbf{m}_0 = \mathbf{m}_0 \cdot \mathbf{C} \cdot \mathbf{m}_0. \tag{2}$$

An analogous procedure follows for other families of fibers defined within the tissue. We shall denote as $\mathbf{n}_0(\mathbf{X})$ a second preferred fiber direction.

In (1), (2) $\mathbf{F} = \partial \boldsymbol{\chi} / \partial \mathbf{X}$ and $\mathbf{C} = \mathbf{F}^T \mathbf{F}$ are the standard deformation gradient and the corresponding right Cauchy–Green tensor, respectively. A multiplicative decomposition of $\mathbf{F}$ into *volume-changing (dilational)* and *volume-preserving (distortional)* parts is usually established, as e.g. in Flory (1961), Ogden (1978)

$$\mathbf{F} = J^{\frac{1}{3}} \bar{\mathbf{F}}, \qquad \mathbf{C} = J^{\frac{2}{3}} \bar{\mathbf{C}}. \tag{3}$$

For isothermal and reversible processes, we postulate the existence of a unique decoupled representation of the strain–energy function (SEF) Ψ (Simo and Taylor, 1985). Because of the directional dependence on the material behavior, we require that the function Ψ depends on both the right Cauchy–Green tensor $\mathbf{C}$ and the fiber directions $\mathbf{m}_0$ and $\mathbf{n}_0$ in the reference configuration. Since Ψ has to be independent of the sign of $\mathbf{m}_0$ and $\mathbf{n}_0$, Ψ must be an even function of these vector fields and so it may be expressed by $\Psi = \Psi(\mathbf{C}, \mathbf{M}, \mathbf{N})$ where $\mathbf{M} = \mathbf{m}_0 \otimes \mathbf{m}_0$ and $\mathbf{N} = \mathbf{n}_0 \otimes \mathbf{n}_0$ are structural tensors (e.g. Weiss et al., 1996). Based on the kinematic description (3), the free energy function for isochoric processes can be written in the decoupled form as

$$\Psi(\mathbf{C}, \mathbf{M}, \mathbf{N}) = \Psi_{\text{vol}}(J) + \bar{\Psi}(\bar{\mathbf{C}}, \mathbf{M}, \mathbf{N}), \tag{4}$$

where $\Psi_{\text{vol}}(J)$ and $\bar{\Psi}(\bar{\mathbf{C}}, \mathbf{M}, \mathbf{N})$ are purely volumetric and isochoric contributions to the material response, respectively (Holzapfel, 2000). In terms of the strain invariants, Spencer (1954), Ψ can be written as

$$\Psi = \Psi_{\text{vol}}(J) + \bar{\Psi}(\bar{I}_1(\bar{\mathbf{C}}), \bar{I}_2(\bar{\mathbf{C}}), \bar{I}_4(\bar{\mathbf{C}}, \mathbf{m}_0), \bar{I}_5(\bar{\mathbf{C}}, \mathbf{m}_0), \bar{I}_6(\bar{\mathbf{C}}, \mathbf{n}_0), \bar{I}_7(\bar{\mathbf{C}}, \mathbf{n}_0), \bar{I}_8(\bar{\mathbf{C}}, \mathbf{m}_0, \mathbf{n}_0), \bar{I}_9(\mathbf{m}_0, \mathbf{n}_0)), \tag{5}$$

with $\bar{I}_1$ and $\bar{I}_2$ the first two modified strain invariants of $\bar{\mathbf{C}}$ (note that $I_3 = J$ and $\bar{I}_3 = 1$). Finally, the pseudo-invariants $\bar{I}_4, \ldots, \bar{I}_9$ characterize the constitutive response of the fibers (Spencer, 1954):

$$\begin{aligned} \bar{I}_4 &= \bar{\mathbf{C}} : \mathbf{M}, \quad \bar{I}_5 = \bar{\mathbf{C}}^2 : \mathbf{M}, \\ \bar{I}_6 &= \bar{\mathbf{C}} : \mathbf{N}, \quad \bar{I}_7 = \bar{\mathbf{C}}^2 : \mathbf{N}, \\ \bar{I}_8 &= (\mathbf{m}_0 \cdot \mathbf{n}_0) \mathbf{m}_0 \cdot \bar{\mathbf{C}} \mathbf{n}_0, \quad \bar{I}_9 = (\mathbf{m}_0 \cdot \mathbf{n}_0)^2. \end{aligned} \tag{6}$$

While the invariants $\bar{I}_4$ and $\bar{I}_6$ are directly identified as the square of the stretch in the fiber directions, the influence of $\bar{I}_5$, $\bar{I}_7$ and $\bar{I}_8$ is difficult to evaluate due to the high correlation among them. For this reason and the lack of sufficient experimental data, it is common to neglect the effect of these invariants in the definition of Ψ

(Weiss et al., 1996; Holzapfel et al., 2000). Finally, $\bar{I}_9$ does not depend of the deformation and, therefore, is not relevant to the constitutive behavior.

Once defined the SEF, the constitutive equation for compressible hyperelastic materials in the standard form is given by

$$\mathbf{S} = 2\frac{\partial \Psi(\mathbf{C},\mathbf{M},\mathbf{N})}{\partial \mathbf{C}} = \mathbf{S}_{\text{vol}} + \bar{\mathbf{S}}, \tag{7}$$

where the second Piola–Kirchhoff stress $\mathbf{S}$ consists of a purely volumetric contribution, $\mathbf{S}_{\text{vol}}$, and a purely isochoric one, $\bar{\mathbf{S}}$. The associated decoupled elasticity tensor may be written as

$$\mathbb{C} = \mathbb{C}_{\text{vol}} + \bar{\mathbb{C}} = 2\frac{\partial \mathbf{S}_{\text{vol}}}{\partial \mathbf{C}} + 2\frac{\partial \bar{\mathbf{S}}}{\partial \mathbf{C}}. \tag{8}$$

The Cauchy stress tensor $\boldsymbol{\sigma}$ and the spatial description of the elasticity tensor, $\mathbb{C}$, are given by the weighted push-forward of $\mathbf{S}$ and $\mathbb{C}$, respectively (Marsden and Hughes, 1994; Holzapfel, 2000)

$$\boldsymbol{\sigma} = J^{-1}\boldsymbol{\chi}_*(\mathbf{S}), \qquad {}_{\mathbb{C}} = J^{-1}\boldsymbol{\chi}_*(\mathbb{C}). \tag{9}$$

For a more detailed derivation of the material and spatial elasticity tensors for compressible or incompressible fibrous hyperelastic materials, and their explicit expressions, see e.g. Weiss et al. (1996) or Holzapfel (2000).

The section that follows presents three-dimensional, rate-independent finite strain damage models to describe the loss in the mechanical stiffness in soft tissues for strains beyond the physiological range. The models are formulated within the framework of non-linear continuum damage mechanics and use the concept of internal variables (Simo and Ju, 1987a,b). Both models are phenomenological, though structural, and describe the macroscopic constitutive behavior for stresses assuming separated contributions of the matrix and the fibers. Therefore, the SEF will be assumed to be of the form

$$\Psi(\mathbf{C},\mathbf{M},\mathbf{N}) = \Psi_{\text{vol}}(J) + \bar{\Psi}^m(\bar{\mathbf{C}}) + \bar{\Psi}^f(\bar{\mathbf{C}},\mathbf{M},\mathbf{N}). \tag{10}$$

3. Damage models for biological soft tissue components

In this section two damage models for the fibrous part of the tissue are described: (i) a continuous damage model, and (ii) a stochastic damage model. The continuous damage model has been recently proposed by Calvo et al. (2006) in which damage in the fibers is described following the same model proposed for the ground material. In contrast, the stochastic model recently proposed in Rodríguez et al. (2006) assumes elastic fibers to behave following a worm-like chain model with a statistical distribution of the fiber length. In this model, individual fiber failure occurs whenever the fiber stretch reaches a threshold value dependent on the fiber length.

3.1. Continuum damage model

In the continuum damage model the free energy for the fibers is assumed to be of the forms

$$\begin{aligned}\bar{\Psi}^f(\bar{\mathbf{C}},\mathbf{M},\mathbf{N}) &= \bar{\Psi}^f_M(\bar{\mathbf{C}},\mathbf{M}) + \bar{\Psi}^f_N(\bar{\mathbf{C}},\mathbf{N}) \\ &= (1-D^M_f)\bar{\Psi}^f_0(\bar{\mathbf{C}},\mathbf{M}) + (1-D^N_f)\bar{\Psi}^f_0(\bar{\mathbf{C}},\mathbf{N}),\end{aligned} \tag{11}$$

where $\bar{\Psi}^f_0$ denotes the isochoric effective strain–energy function of the undamaged fibers. The internal variables $D^N_f, D^M_f \in [0,1]$ are referred to as the damage variables for the fibers. In what follows we will focus the development in one family of fibers, since results are identical for the other family.

The time rate of change of (11) is found to be, after using the chain rule,

$$\dot{\bar{\Psi}}^f_M = (1-D^M_f)\frac{\partial \bar{\Psi}^f_0(\bar{\mathbf{C}},\mathbf{M})}{\partial \bar{\mathbf{C}}} : \dot{\bar{\mathbf{C}}} - \bar{\Psi}^f_0(\bar{\mathbf{C}},\mathbf{M})\dot{D}^M_f. \tag{12}$$

Particularization of the Clausius–Planck inequality leads to the non-negative internal dissipation $\mathcal{D}_{\text{int}}$ (Neto et al., 1998)

$$\mathcal{D}_{\text{int}}^{fM} = \left[\bar{\mathbf{S}}^{fM} - J^{-\frac{2}{3}}\mathbb{P} : (1 - D_f^M) 2 \frac{\partial \bar{\Psi}_0^f(\bar{\mathbf{C}}, \mathbf{M})}{\partial \bar{\mathbf{C}}}\right] : \frac{\dot{\bar{\mathbf{C}}}}{2} + \bar{\Psi}_0^f \dot{D}_f^M \geqslant 0, \tag{13}$$

where $\mathbb{P} = \mathbb{I} - \frac{1}{3}\bar{\mathbf{C}}^{-1} \otimes \bar{\mathbf{C}}^{-1}$ is the fourth-order projection tensor.

Using standard arguments in continuum constitutive mechanics, the isochoric second Piola–Kirchhoff stress $\bar{\mathbf{S}}^{fM}$ may be written as

$$\bar{\mathbf{S}}^{fM} = (1 - D_f^M)\bar{\mathbf{S}}_0^{fM} \tag{14}$$

with

$$\bar{\mathbf{S}}_0^{fM} = 2J^{-\frac{2}{3}}\mathbb{P} : \frac{\partial \bar{\Psi}_0^f(\bar{\mathbf{C}}, \mathbf{M})}{\partial \bar{\mathbf{C}}}, \tag{15}$$

and from the same arguments

$$\mathcal{D}_{\text{int}}^{fM} = f_f^M \dot{D}_f^M \geqslant 0, \tag{16}$$

with

$$f_f^M = \bar{\Psi}_0^f(\bar{\mathbf{C}}, \mathbf{M}) \geqslant 0. \tag{17}$$

Inequality (16) clearly shows that damage is a dissipative process. The quantity f_f^M denotes the thermodynamic driving force which governs the damage evolution of the family of fibers defined by the structural tensor $\mathbf{M}$, and has the meaning of the effective strain energy, $\bar{\Psi}_0^f(\mathbf{C}, \mathbf{M})$, of the corresponding family. f_f^M is conjugate of the internal variable D_f^M

$$f_f^M = \bar{\Psi}_0^f(\bar{\mathbf{C}}, \mathbf{M}) = -\frac{\partial \bar{\Psi}_M^f}{\partial D_f^M}. \tag{18}$$

3.1.1. Evolution of damage

The evolution of the damage parameter D_f^M is characterized by an irreversible equation as given by (16). Following Simo (1987), let

$$\Xi_s^{fM} = \sqrt{2\bar{\Psi}_0^{fM}(\bar{\mathbf{C}}(s), \mathbf{M})}, \tag{19}$$

where $\bar{\mathbf{C}}(s)$ is the modified right Cauchy–Green tensor at time s. Now, let Ξ_t^{fM} be the maximum value of Ξ_s^{fM} over the past history up to current time t, that is

$$\Xi_t^{fM} = \max_{s \in (-\infty, t)} \sqrt{2\bar{\Psi}_0^{fM}(\bar{\mathbf{C}}(s), \mathbf{M})}. \tag{20}$$

The feasible strain space for the fibers is defined as the condition that, at any time t of the loading process, the following expression is fulfilled (Simo, 1987),

$$\phi^{fM}(\mathbf{C}(t), \Xi_t^{fM}) = \sqrt{2\bar{\Psi}_0^{fM}(\bar{\mathbf{C}}(t), \mathbf{M})} - \Xi_t^{fM} \leqslant 0. \tag{21}$$

The equation $\phi^{fM}(\bar{\mathbf{C}}(t), \Xi_t^{fM}) = 0$ defines a damage surface in the strain space. Denoting by $T_f^M := \partial\phi^{fM}/\partial\bar{\mathbf{C}}$, the normal to the damage surface in that space, the following alternative situations may occur:

$$\phi^{fM} < 0 \quad \text{or} \quad \phi^{fM} = 0 \quad \text{and} \quad \begin{cases} \mathbf{T}_f^M : \delta\bar{\mathbf{C}} < 0, \\ \mathbf{T}_f^M : \delta\bar{\mathbf{C}} = 0, \\ \mathbf{T}_f^M : \delta\bar{\mathbf{C}} > 0, \end{cases} \tag{22}$$

where $\delta\bar{\mathbf{C}}$ is an arbitrary admissible variation of $\bar{\mathbf{C}}$. Borrowing a terminology typically found in plasticity (Simo and Hughes, 1998; Naghdi and Trapp, 1975), we speak of unloading, neutral loading, or loading from a damage state, respectively. Finally, the evolution of the damage variable D_f^M is specified by the irreversible rate equation

$$\frac{\mathrm{d}D_f^M}{\mathrm{d}t} = \begin{cases} \bar{h}_f^M(\Xi^{fM}, D_f^M)\dot{\Xi}^{fM} & \text{if} \quad \phi^{fM} = 0 \quad \text{and} \quad \mathbf{T}_f^M : \dot{\bar{\mathbf{C}}} > 0, \\ 0 & \text{otherwise.} \end{cases} \tag{23}$$

Here $\bar{h}_f^M(\Xi^{fM}, D_f^M)$ is a given function that characterizes damage evolution in the material. If $\bar{h}_f^M(\Xi^{fM}, D_f^M)$ is independent of D_f^M, the deviatoric part of the second Piola–Kirchoff stress tensor for the matrix may be expressed in the following form

$$\bar{\mathbf{S}}^{fM}(t) = \bar{g}_f(\Xi_t^{fM}) 2 \frac{\partial \bar{\Psi}_0^f(\bar{\mathbf{C}}(t), \mathbf{M})}{\partial \mathbf{C}} = \bar{g}_f(\Xi_t^{fM}) \bar{\mathbf{S}}_0^{fM}(\bar{\mathbf{C}}(t), \mathbf{M}), \tag{24}$$

with $\bar{h}_f^M(\Xi^{fM}) = -\mathrm{d}\bar{g}_f(\Xi^{fM})/\mathrm{d}\Xi^{fM}$.

To completely determine the damage model, it still remains to specify the function $\bar{g}_f(\Xi^{fM})$, or equivalently, the function $\bar{h}_f^M$. Such a determination should be made on the basis of available experimental data.

3.2. Stochastic damage model

Histological studies performed in a number of soft tissues (Sacks et al., 1994; Canham et al., 1997; Hsu et al., 1998; Dingemans et al., 2000) have shown that elastic fibers appear to be wavy and distributed about preferential directions, Lanir (1983). Thus, as the load is applied, more and more fibers start to bear load. However, the degree of straightening of each fiber will also depend upon its orientation relative to the loading and the interstitial matter which might avoid the complete straightening of the fibers as suggested by Samila and Carter (1981). In their work, they also found that collagen fibers straighten more at large strains, while elastin lamellae unfolded quickly with initial stretch. The model here presented treats the wavy nature of elastic fibers, as proposed by Rodríguez et al. (2006), where they are assumed to behave following a worm-like chain model (Arruda and Boyce, 1993). The model does not consider any constraint imposed by the interstitial matter over the deformation of the fibers, keeping the fully uncoupled nature of the original model. In what follows, the fibrous part is considered to be composed of oriented bundles of fibers which can be grouped in two families of elastic fibers. Therefore, it is first characterized the mechanical behavior of a bundle, and later, bundle orientation is incorporated through the definition of the two families of fibers (defined by $\mathbf{m}_0(\mathbf{X})$ and $\mathbf{n}_0(\mathbf{X})$).

3.2.1. Fiber bundles

Each bundle of fibers is assumed to behave following the eight-chain model proposed by Arruda and Boyce (1993) and particularized for the case of transversally isotropic materials, i.e.,

$$\bar{\Psi}_{\mathrm{coll}}(\lambda) = D_1 \left[2\frac{r_0^2}{L^2}\lambda^2 + \frac{1}{1-\frac{r_0}{L}\lambda} - \frac{r_0}{L}\lambda\left(4\frac{r_0}{L} + \frac{1}{(1-\frac{r_0}{L})^2} - 1\right)\frac{r_0}{2L}\ln(\lambda^2)\right] - \bar{\Psi}^r_{\mathrm{coll}}, \tag{25}$$

with D_1 a material constant, L the maximum fiber length, $r_0 < L$ a reference fiber length, λ the actual fiber stretch, and

$$\bar{\Psi}^r_{\mathrm{coll}} = 2\frac{r_0^2}{L^2} + \frac{1}{1-\frac{r_0}{L}} - \frac{r_0}{L}, \tag{26}$$

a repository strain–energy that guarantees $\bar{\Psi}_{\mathrm{coll}}(1) = 0$. This model considers the maximum fiber length, L, as a Beta random variable, and assumes the same average orientation for all fibers within the bundle as well as that fibers do not bear compressive loads. Hence, the SEF for a bundle of fibers is given by

$$\bar{\Psi}_{\text{bund}}(\lambda,\lambda_t^m)=\begin{cases}0, & \lambda<1,\\ \int_1^{\lambda}\int_{a(r_0\lambda_t^m)}^{\kappa}\sigma_{\text{coll}}(\xi,x)f_L(x)\mathrm{d}x\mathrm{d}\xi, & \lambda\geqslant 1,\end{cases} \tag{27}$$

where $a(r_0\lambda_t^m)$ is a monotonically increasing function that determines the minimal fiber length within the bundle for which failure has not yet occurred, $\sigma_{\text{coll}}\equiv\partial\bar{\Psi}_{\text{coll}}/\partial\lambda$ and $f_L(x)$ is a Beta probability density function with parameters γ and η

$$f_L(x)=\frac{1}{\kappa-r_0}\frac{\Gamma(\eta+\gamma)}{\Gamma(\eta)\Gamma(\gamma)}\left(\frac{x-r_0}{\kappa-r_0}\right)^{\gamma-1}\left(1-\frac{x-r_0}{\kappa-r_0}\right)^{\eta-1},\quad x\in[r_0,\kappa]. \tag{28}$$

The parameter λ_t^m in (27) corresponds to the maximum fiber stretch attained by the bundle over the past history up to time $t\in\mathcal{R}_+$. Therefore, the damage of the fiber bundle increases whenever $\lambda_t-\lambda_t^m\geqslant 0$, and it is strain driven. On the other hand, function $a(r_0\lambda_t^m)$ is taken to be

$$a(r_0\lambda_t^m)=\exp\left[\left(\frac{r_0\lambda_t^m}{\delta}\right)^{\theta}\right]r_0\lambda_t^m, \tag{29}$$

where θ and δ are model parameters. Note that with this form of $a(r_0\lambda_t^m)$, the bundle will degrade faster as the deformation gets larger (i.e., longer fibers will fail at a smaller fraction of their maximum length).

Note that, at the fiber level, this model differs from that proposed by Hurschler et al. (1997) in which the fiber bundle is assumed to be linearly elastic and wavy with constant rupture energy (e.g., all fibers fail when they reach a given limit strain). In this model the bundle is an assembly of fibers with a different strain–energy at fracture. In addition, the fact that the Beta distribution is bounded ensures that the probability of a fiber bundle failure at 0 strain is 0 as well as for fiber bundles strained above the distribution limit κ.

3.2.2. Oriented fiber bundles

Eq. (27) defines the strain–energy for fiber bundles when stretched along their longitudinal axis. In a general fibrous soft tissue, for a family of fibers aligned along a preferred direction $\mathbf{m}_0$, the fiber stretch at time s, λ_s^M is given as

$$\lambda_s^M=\sqrt{\mathbf{M}:\bar{\mathbf{C}}(s)}\equiv\sqrt{\bar{I}_4(s)}, \tag{30}$$

and the maximum stretch over the past history is according to

$$\lambda_t^{Mm}=\max_{0\leqslant s\leqslant t}\{\lambda_s^M\}. \tag{31}$$

The non-increasing damage criterion in the strain space is given by the condition that

$$\varphi_f^M(\bar{\mathbf{C}}(t),\lambda_t^{Mm}):=\lambda_t^M-\lambda_t^{Mm}\leqslant 0,\quad\forall t\in\mathcal{R}_+, \tag{32}$$

where $\varphi_f^M(\bar{\mathbf{C}}(t),\lambda_t^{Mm})=0$ defines a damage surface in the strain space with normal $\mathbf{T}_f^M:=\partial\varphi_f^M/\partial\bar{\mathbf{C}}\equiv\mathbf{M}/(2\lambda_t^M)$, and the damaging criterion follows (22). Hence, the anisotropic component of the strain–energy function associated with this family of fibers is

$$\bar{\Psi}_M^f(\bar{I}_4(t),\lambda_t^{Mm})=\bar{\Psi}_{\text{bund}}(\sqrt{\bar{I}_4(t)},\lambda_t^{Mm}). \tag{33}$$

The second Piola–Kirchhoff stress tensor at time t, $\bar{\mathbf{S}}^{fM}(\bar{\mathbf{C}}(t),\lambda_t^{Mm})$, is then

$$\bar{\mathbf{S}}^{fM}(\bar{\mathbf{C}}(t),\lambda_t^{Mm})=\begin{cases}2J^{-2/3}\mathbb{P}:\left(\frac{\partial\bar{\Psi}_M^f(\bar{I}_4,\lambda_t^{Mm})}{\partial\bar{\mathbf{C}}}\right), & \text{if}\quad\lambda_t^M\geqslant 1,\\ 0, & \text{otherwise.}\end{cases} \tag{34}$$

The Cauchy stress tensor is found by the weighted push-forward operation (9) of the previous expression. Equivalent expressions for the second family of fibers are obtained by replacing $\bar{I}_4$ by $\bar{I}_6:=\mathbf{N}:\bar{\mathbf{C}}$.

3.3. Damage model for the matrix

Damage in the matrix is assumed to affect only the isochoric elastic part of the deformation, as proposed by Simo (1987). Hence, the free-energy function for the matrix can be written as

$$\bar{\Psi}^m(\bar{\mathbf{C}}) = (1 - D_m)\bar{\Psi}_0^m(\bar{\mathbf{C}}), \tag{35}$$

where $\bar{\Psi}_0^m$ denotes the isochoric effective strain–energy function of the undamaged material, which describes the elastic response of the matrix. The factor $(1 - D_m)$ is known as the reduction factor (Simo, 1987), where the internal variable $D_m \in [0,1]$ is a normalized scalar referred to as the damage variable for the matrix. The evolution of the damage parameter and subsequent determination of stress tensors are described using the concepts discussed in Section 3.1.

4. Decoupled representation of the elasticity tensor

An SEF of the form (10) allows for a decoupled representation of the material elasticity tensor as

$$\mathbb{C} = \mathbb{C}_{\text{vol}} + \bar{\mathbb{C}}^m + \bar{\mathbb{C}}^f, \tag{36}$$

where $\mathbb{C}_{\text{vol}}$ is given by the expression

$$\mathbb{C}_{\text{vol}} = pJ(\mathbf{C}^{-1} \otimes \mathbf{C}^{-1} + 2\mathbb{I}_{\mathbf{C}^{-1}}), \tag{37}$$

with $(\mathbb{I}_{\mathbf{C}^{-1}})_{IJKL} = -1/2(\mathbf{C}^{-1}_{IK}\mathbf{C}^{-1}_{JL} + \mathbf{C}^{-1}_{IL}\mathbf{C}^{-1}_{JK})$ and $\bar{\mathbb{C}}^m$ may be obtained by applying the time derivative to the stress tensor (24). Making use of the chain rule we have (Holzapfel, 2000)

$$\dot{\bar{\mathbf{S}}}^m = \bar{\mathbb{C}}^m : \frac{\dot{\mathbf{C}}}{2} = \begin{cases} [\bar{g}_m \bar{\mathbb{C}}_0^m - \bar{g}'_m \bar{\mathbf{S}}_0^m \otimes \bar{\mathbf{S}}_0^m] : \frac{\dot{\mathbf{C}}}{2}, & \text{if} \quad \phi = 0 \quad \text{and} \quad \mathbf{T}_m : \dot{\mathbf{C}} > 0, \\ \bar{g}_m \bar{\mathbb{C}}_0^m : \frac{\dot{\mathbf{C}}}{2}, & \text{otherwise}, \end{cases} \tag{38}$$

with $\bar{g}'_m = \mathrm{d}\bar{g}_m/\mathrm{d}\Xi^m = -\bar{h}_m$.

For the contribution of the fibers we must distinguish between the continuum and stochastic models. For the continuum model, the elasticity tensor has a similar expression as the one for the matrix

$$\dot{\bar{\mathbf{S}}}^f = \bar{\mathbb{C}}^f : \frac{\dot{\mathbf{C}}}{2} = \begin{cases} [\bar{g}_f \bar{\mathbb{C}}_0^f - \bar{g}'_f \bar{\mathbf{S}}_0^f \otimes \bar{\mathbf{S}}_0^f] : \frac{\dot{\mathbf{C}}}{2}, & \text{if} \quad \phi = 0 \quad \text{and} \quad \mathbf{T}_f : \dot{\mathbf{C}} > 0, \\ \bar{g}_f \bar{\mathbb{C}}_0^f : \frac{\dot{\mathbf{C}}}{2}, & \text{otherwise}, \end{cases} \tag{39}$$

and $\bar{g}'_f = \mathrm{d}\bar{g}_f/\mathrm{d}\Xi^f = -\bar{h}_f$.

For the stochastic model, we express $\bar{\mathbb{C}}^f$ as

$$\bar{\mathbb{C}}^f = \bar{\mathbb{C}}^{fM} + \bar{\mathbb{C}}^{fN}, \tag{40}$$

with

$$\begin{aligned} \bar{\mathbb{C}}^{fM} \;=\; & \tfrac{4}{9}J^{-4/3}(\bar{I}_4\bar{\Psi}_4 + \bar{I}_4^2\bar{\Psi}_{44})\bar{\mathbf{C}}^{-1} \otimes \bar{\mathbf{C}}^{-1} \\ & - \tfrac{4}{3}J^{-4/3}(\bar{\Psi}_4 + \bar{I}_4\bar{\Psi}_4)(\mathbf{M} \otimes \bar{\mathbf{C}}^{-1} - \tfrac{1}{3}\bar{\mathbf{C}}^{-1} \otimes \mathbf{M}) \\ & - \tfrac{4}{3}J^{-4/3}\bar{I}_4\bar{\Psi}_4\mathbb{I}_{\bar{\mathbf{C}}^{-1}} + 4J^{-4/3}\bar{\Psi}_{44}\mathbf{M} \otimes \mathbf{M}, \end{aligned} \tag{41}$$

and

$$\begin{aligned} \bar{\mathbb{C}}^{fN} \;=\; & \tfrac{4}{9}J^{-4/3}(\bar{I}_6\bar{\Psi}_6 + \bar{I}_6^2\bar{\Psi}_{66})\bar{\mathbf{C}}^{-1} \otimes \bar{\mathbf{C}}^{-1} \\ & - \tfrac{4}{3}J^{-4/3}(\bar{\Psi}_6 + \bar{I}_6\bar{\Psi}_6)(\mathbf{N} \otimes \bar{\mathbf{C}}^{-1} - \tfrac{1}{3}\bar{\mathbf{C}}^{-1} \otimes \mathbf{N}) \\ & - \tfrac{4}{3}J^{-4/3}\bar{I}_6\bar{\Psi}_6\mathbb{I}_{\bar{\mathbf{C}}^{-1}} + 4J^{-4/3}\bar{\Psi}_{66}\mathbf{N} \otimes \mathbf{N}, \end{aligned} \tag{42}$$

where $\bar{\Psi}_4 = \partial\bar{\Psi}^f/\partial\bar{I}_4$, $\bar{\Psi}_6 = \partial\bar{\Psi}^f/\partial\bar{I}_6$, $\bar{\Psi}_{44} = \partial^2\bar{\Psi}^f/\partial\bar{I}_4^2$, and $\bar{\Psi}_{66} = \partial^2\bar{\Psi}^f/\partial\bar{I}_6^2$. Expressions for $\bar{\Psi}_4$, and $\bar{\Psi}_{44}$ are given below. Thus,

$$\bar{\Psi}_4(\lambda_t^M,\lambda_t^{Mm})=\begin{cases}0, & \text{if } \lambda_t^M<1,\\ \frac{1}{2\lambda_t^M}\int_{a(r_0\lambda_t^{Mm})}^{\kappa}\sigma_{\text{coll}}(\lambda_t^M,x)f_L(x)\mathrm{d}x, & \text{if } \lambda_t^M\geqslant 1,\end{cases}\tag{43}$$

where $a(r_0\lambda_t^{Mm})$ is given in (29). For the second derivative with respect to $\bar{I}_4$, $\bar{\Psi}_{44}$, we have

$$\bar{\Psi}_{44}(\lambda_t^M,\lambda_t^{Mm})=\begin{cases}\Psi_{44}^L(\lambda_t^M,\lambda_t^{Mm}), & \text{if } \lambda_t^M\geqslant\lambda_t^{Mm},\\ \Psi_{44}^U(\lambda_t^M,\lambda_t^{Mm}), & \text{if } \lambda_t^M<\lambda_t^{Mm},\\ 0, & \text{otherwise},\end{cases}\tag{44}$$

where

$$\bar{\Psi}_{44}^U(\lambda_t^M,\lambda_t^{Mm})=\frac{1}{4(\lambda_t^M)^2}\int_{a(r_0\lambda_t^{Mm})}^{\kappa}\left[\frac{1}{\lambda_t^M}\sigma'_{\text{coll}}(\lambda_t^M,x)-\sigma_{\text{coll}}(\lambda_t^M,x)\right]f_L(x)\mathrm{d}x,\tag{45}$$

with $\sigma'_{\text{coll}}(\lambda,x)=\partial\sigma_{\text{coll}}(\lambda,x)/\partial\lambda$, and

$$\bar{\Psi}_{44}^L(\lambda_t^M,\lambda_t^M)=\bar{\Psi}_{44}^U(\lambda_t^M,\lambda_t^M)-\frac{1}{4(\lambda_t^M)^2}\sigma_{\text{coll}}(\lambda_t^M,a(r_0\lambda_t^M))f_L(a(r_0\lambda_t^M))\frac{\partial a(r_0\lambda)}{\partial\lambda}|_{\lambda=\lambda_t^M}.\tag{46}$$

The spatial description of the elasticity tensor is obtained by the weighted push forward of (36) given by Eq. (9). Close form expressions for the spatial versions of the elasticity tensor are omitted for simplicity.

5. Examples

The damage models proposed above have been implemented in ABAQUS 6.5-1 through appropriate UMAT Fortran subroutines.

In all examples, the proposed damage functions for matrix and fibers in the continuum model are given by

$$\bar{g}_m(\Xi_t^m)=\begin{cases}1, & \text{if } \Xi_t^m<\psi_{\min}^m,\\ 1-\left[1-\beta^m+\beta^m\left(\frac{\Xi_t^m-\psi_{\min}^m}{\psi_{\min}^m-\psi_{\max}^m}\right)^2\right]\left(\frac{\Xi_t^m-\psi_{\min}^m}{\psi_{\min}^m-\psi_{\max}^m}\right)^2, & \text{if } \psi_{\min}^m\leqslant\Xi_t^m\leqslant\psi_{\max}^m,\\ 0, & \text{if } \Xi_t^m>\psi_{\max}^m,\end{cases}\tag{47}$$

$$\bar{g}_f(\Xi_t^f)=\begin{cases}1, & \text{if } \Xi_t^f<\psi_{\min}^f,\\ 1-\left[1-\beta^f+\beta^f\left(\frac{\Xi_t^f-\psi_{\min}^f}{\psi_{\min}^f-\psi_{\max}^f}\right)^2\right]\left(\frac{\Xi_t^f-\psi_{\min}^f}{\psi_{\min}^f-\psi_{\max}^f}\right)^2, & \text{if } \psi_{\min}^f\leqslant\Xi_t^f\leqslant\psi_{\max}^f,\\ 0, & \text{if } \Xi_t^f>\psi_{\max}^f,\end{cases}\tag{48}$$

where $\psi_{\min}^m$ and $\psi_{\min}^f$ are the strain energies at the initial damage for matrix and fibers, respectively, $\psi_{\max}^m$ and $\psi_{\max}^f$ are the strain energies at maximum damage for matrix and fibers, and β^m and β^f the exponential parameters for matrix and fibers, respectively (Natali et al., 2005; Simo, 1987).

In addition, the volumetric part of the strain–energy function has been treated via a penalty method within the ABAQUS formulation. The penalty function has been chosen to be $\Psi_{\text{vol}}(J)=(1/D)(J-1)^2$, with $D=1E-5$ for all simulations. For the matrix, the deviatoric function (49) has been used in both models. Expression (50), taken from Holzapfel et al. (2000), has been assumed for each family of fibers in the continuum model

$$\bar{\Psi}_0^m=C_1(\bar{I}_1-3)+C_2(\bar{I}_2-3),\tag{49}$$

$$\bar{\Psi}_0^f(\bar{\mathbf{C}},\mathbf{A})=\frac{C_3}{2C_4}(\exp^{C_4(\bar{\mathbf{C}}:\mathbf{A}-1)^2}-1).\tag{50}$$

For the stochastic model, fiber damage will be quantified as

$$D_f = \text{Beta}\left[\frac{a(r_0\lambda_t^m) - r_0}{\kappa - r_0}, \gamma, \eta\right], \tag{51}$$

where Beta[·] is the incomplete Beta function, and $r_0 = 1.215$ for all calculations. Note that this corresponds to the cumulative probability function of L measured in terms of $a(r_0\lambda_t^m)$. In other words, $D_f = 0.8$ says that there is an 80% probability of having all fibers broken for a bundle stretch λ_t^m.

5.1. Uniaxial test: analytical example

This example considers a single finite element simulation of a uniaxial test along the collagen fiber direction (only one family of fibers is considered) under displacement control. Material and damage parameters have been taken to be that of a medium collateral ligament (MCL), and models have been calibrated with experimental results reported in Weiss (1994). Damage parameters have been adjusted to capture the drop in the stress–stretch curve, while elastic constants have been adjusted to capture the response at small stretch values and subsequent rapid stiffening. The numerical fit of both models to experimental data in Weiss (1994) is depicted in Fig. 1. Tables 1 and 2 show the numerical values for the parameters.

Fig. 2 shows the response of both models to cyclic loading. From the figure it can be observed that both models are able to describe the typical Mullins' effect. Note, however, that the stiffness loss is not the same in both models. A slightly larger stiffness loss appears to be associated with the stochastic model, even though both of them describe the same primary loading path (the one traced if there were no unloading).

Fig. 3 shows the damage functions (48) and (51) for both models. For the stochastic model, damage occurs continuously from the moment fibers start to bear load, while for the continuum model, damage occurs when the fiber energy reaches a given threshold (this threshold can be varied by changing the value of $\psi^f_{\min}$). On the other hand, the stochastic model assumes that the fiber bundle is composed of an array of fibers with different strain–energy to failure (the distribution follows the Beta distribution), while for the continuum model damage does not affect the strain–energy function of the remaining fibers. For the stochastic model, shorter fibers (shorter fibers are also stiffer, see Eq. (25) for larger L) fail first, and therefore, the model predicts a fast load bearing capacity lost at large stretch as compared with the continuum model as shown in Fig. 2.

5.2. Stretching of a thin perforated square plate

This example presents the numerical simulation of a thin perforated plate subjected to biaxial stretching. The geometry, boundary conditions and mesh are shown in Fig. 4. Due to the symmetry only one quarter of the plate was considered in the finite element simulation. Two families of fibers defined at $\pm 45^\circ$ with respect to the X direction were considered ($\mathbf{m}_0 = \{\sqrt{2}/2, \sqrt{2}/2, 0.0\}$, $\mathbf{n}_0 = \{\sqrt{2}/2, -\sqrt{2}/2, 0.0\}$). The thin plate is sub-

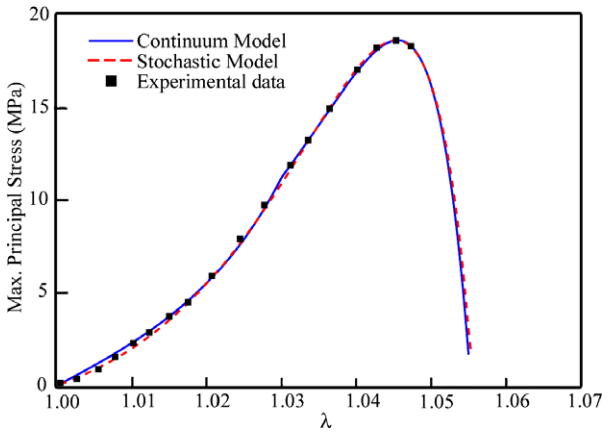

Fig. 1. Continuum and stochastic damage models fitted to experimental data.

Table 1
Material and damage parameters for the continuum model in the uniaxial test

C_1 (MPa)	C_2 (MPa)	C_3 (MPa)	C_4 (–)		
5.05	0.0	46.0	150.2		
$\psi^m_{\min}$ ($\sqrt{\text{MPa}}$)	$\psi^m_{\max}$ ($\sqrt{\text{MPa}}$)	β^m	$\psi^f_{\min}$ ($\sqrt{\text{MPa}}$)	$\psi^f_{\max}$ ($\sqrt{\text{MPa}}$)	β^f
0.1635	0.2974	20	0.4778	1.3342	0.01

The model has been calibrated with data reported in Weiss (1994).

Table 2
Material parameters for the stochastic model as calibrated with experimental data from Weiss (1994)

C_1 (MPa)	C_2 (MPa)	α	β	D_1 (MPa)
5.05	0.0	0.49	5.78	0.011
γ	η	κ	δ	θ
5.07	1.0	1.308	15.1	1.88

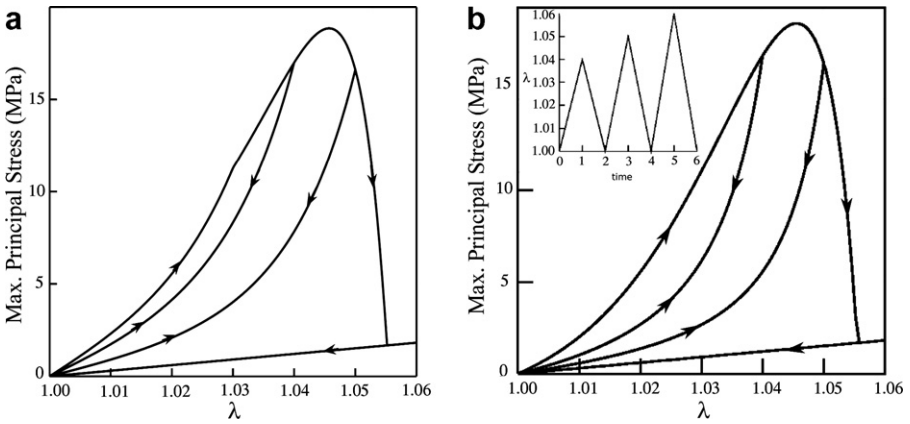

Fig. 2. Model response under cyclic loading: (a) continuum model; (b) stochastic damage model. Strain history for both models is shown in the insert.

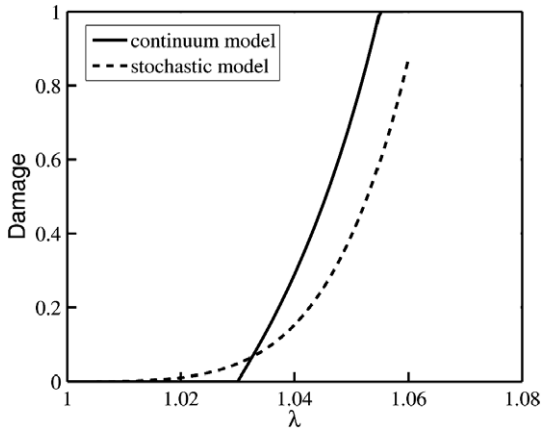

Fig. 3. Evolution of damage for continuum and stochastic models, showing the more gradual evolution for the stochastic model.

jected to an equi-biaxial displacement control experiment. The aim of this numerical experiment is to test both models under biaxial load. Material parameters for both damage models are the same as in the previous example.

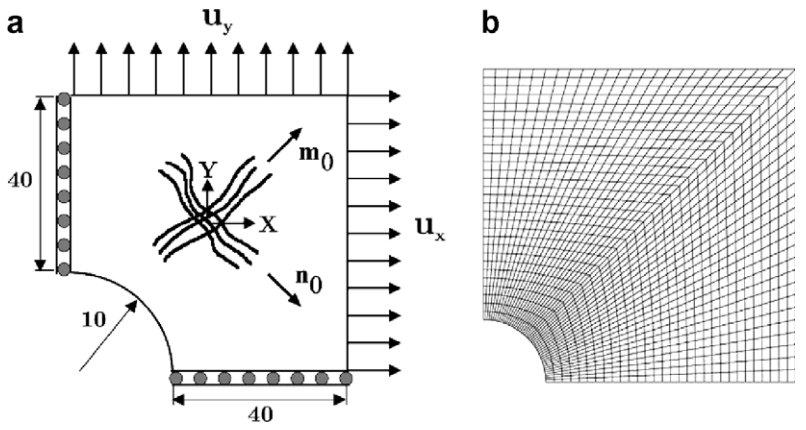

Fig. 4. Thin perforated square plate. Geometry, boundary conditions and mesh.

Figs. 5 and 6 show damage in both families of fibers for the continuum and the stochastic models in the deformed configuration, respectively. A strong damage localization in both models can be observed, however, it appears to be more acute in the continuum damage model. No damage is predicted for the continuum model for the second family of fibers (orientation N_2), while the stochastic model already predicts some damage to occur, even though it is small. This behavior is explained by Fig. 3. While for the stochastic model damage in the tissue occurs continuously as the fiber stretch increases, for the continuous model, damage occurs after a given threshold is reached, at which point damage starts to increase monotonically. Damage localization for continuum and stochastic models occur at the location where maximum fiber stress and stretch are found, respectively, as shown in Fig. 7.

5.3. Damage in arteries after balloon angioplasty

The widespread use of balloon angioplasty has motivated to study the mechanical behavior of arteries at pressures beyond the physiological range. In this regard, Gasser and Holzapfel (2002) developed an elasto-plastic model for biological fibrous tissues and used it to model balloon angioplasty (Holzapfel et al., 2002). Oktay (1993) carried out pressure–volume and extension experiments on bovine coronary arteries finding a reduction in the stiffness of the material after angioplasty, proving that damage was induced by this procedure.

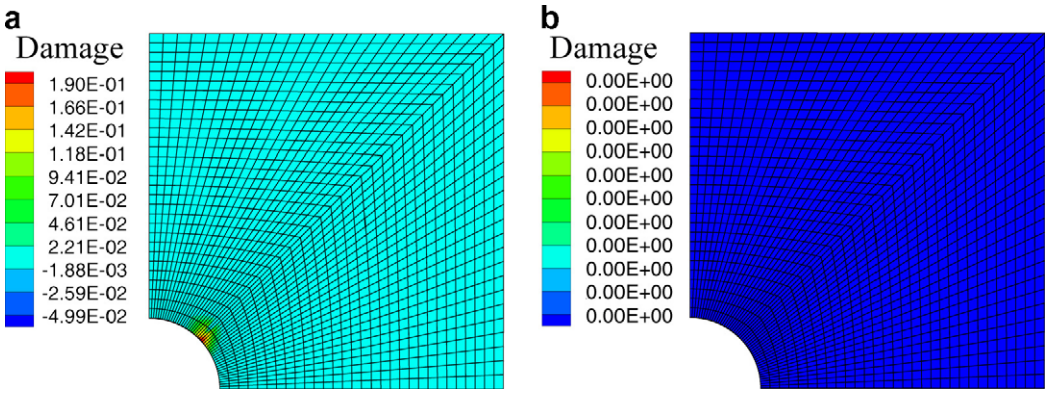

Fig. 5. Damage contours for the two family of fibers for the continuum model: (a) elastic fiber along $\mathbf{n}_0$ direction; (b) elastic fiber along $\mathbf{m}_0$ direction.

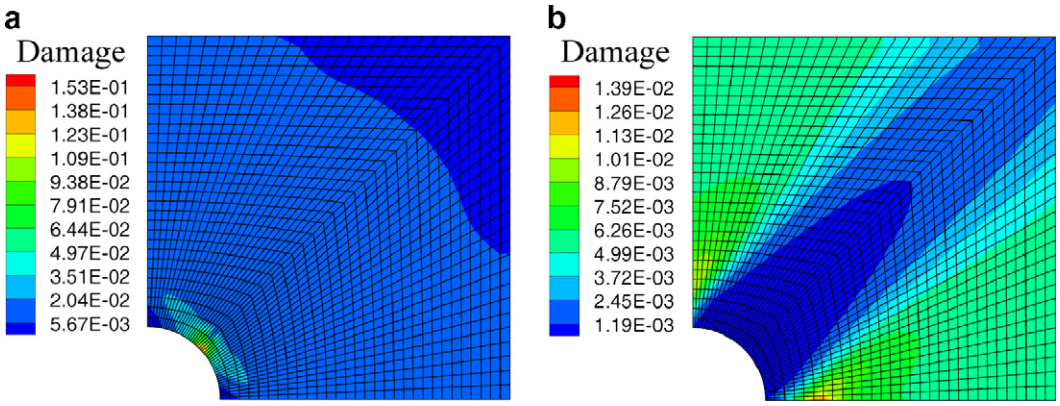

Fig. 6. Damage contours for the two family of fibers for the stochastic model: (a) elastic fiber along $\mathbf{n}_0$ direction; (b) elastic fiber along $\mathbf{m}_0$ direction.

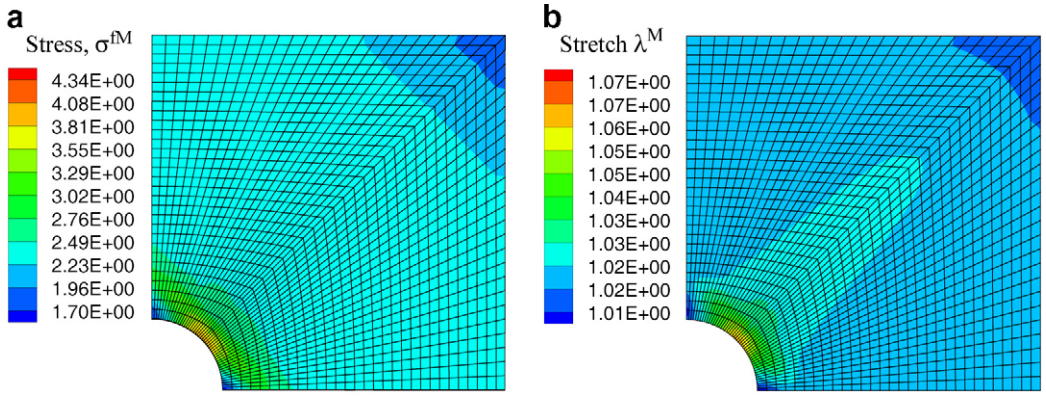

Fig. 7. (a) Fiber stress ($\mathbf{m}_0$ direction) for the continuum model; (b) fiber stretch ($\mathbf{m}_0$ direction) for the stochastic model.

The purpose of this example is to compare both damage models under a more general loading condition in a load control experiment. We will attempt to model Oktay experiments in bovine coronary arteries. The geometry of a healthy left anterior descending coronary artery (LAD) with 40 mm in length, and internal and external diameters $D_i = 2.7$ mm and $D_o = 4.5$ mm, respectively, has been considered. The artery has been simulated as a multi-layered composite material by considering the *media*, and *adventitia* layers within the model (thickness ratio of 1.65:1), and without plaque. The geometry has been discretized by means of 49,280 trilinear incompressible elements. The angle of the fibers with respect to the circumferential direction, ϕ, for both layers is given in Table 3. In addition, initial stress has been accounted for in the simulation by imposing an opening angle of 120° by means of an initial compatible deformation gradient, as proposed by Rodriguez et al. (1994). The axial extension is restrained at both ends while allowing radial expansion.

Table 3
Material and damage parameters for the coronary artery for the continuum model

	C_1 (kPa)	C_2 (kPa)	C_3 (kPa)	C_4	ϕ
Media	27.4	0.0	0.64	3.54	10°
Adventitia	2.7	0.0	5.1	15.4	40°
$\psi^m_{\min}$ ($\sqrt{\text{MPa}}$)	$\psi^m_{\max}$ ($\sqrt{\text{MPa}}$)	β^m	$\psi^f_{\min}$ ($\sqrt{\text{MPa}}$)	$\psi^f_{\max}$ ($\sqrt{\text{MPa}}$)	β^f
6.99	15.0	0.1	3.54	10	0.5

Elastic parameters for the continuum model were taken from Gasser et al. (2002) and damage parameters were obtained by fitting the damage model to data presented in Oktay (1993). For the stochastic model, parameters have been fitted to reproduce the same uniaxial behavior (primary loading path) as the continuum model, following the same procedure as in the uniaxial test problem presented in the first example. Tables 3 and 4 show the material parameters for both models used in this example. Fig. 8 depicts the stress–stretch behavior for both models under uniaxial loading, showing an excellent agreement. We have to point out that damage in the matrix has not been considered in this example, since we were mainly concerned with the damage behavior of the fibers where both models differ substantially.

For the balloon, we have taken a Grüntzig-type balloon catheter. As the initial configuration of the balloon, we have taken a cylindrical tube with external diameter $d = 1.7$ mm, wall-thickness 0.1 mm and length 20 mm. The geometry has been discretized by means of 1000 trilinear incompressible elements.

The material of the balloon has been modeled as a fiber-reinforced composite with fibers running longitudinally and circumferentially, as suggested by Gasser and Holzapfel (2006), i.e.,

$$\Psi(\mathbf{C}, \mathbf{n}_l, \mathbf{n}_c) = U(J) + \frac{c}{2}(\bar{I}_1 - 3) + \sum_{i=l,c} \left\{ \frac{k_{1i}}{k_{2i}} \{\exp[k_{2i}(\lambda_i^2 - 1)^2] - 1\} \right\} \tag{52}$$

where $\mathbf{n}_i$, $i = l, c$, are the directions of the reinforcing fibers and $\lambda_i^2 = \mathbf{n}_i \cdot \mathbf{C} \cdot \mathbf{n}_i$, and $U(J) = \Psi_{\text{vol}}(J)$.

In the model proposed by Gasser and Holzapfel (2006), the two families of fibers are immersed in a soft isotropic matrix, with both families of fibers having different mechanical properties. The circumferentially-oriented fibers are very soft at small strains, getting rapidly stiffer at larger strains. On the other hand, longitudinal fibers are assumed to be already stiff from the beginning. These properties of the material cause small shortening of the balloon, while allowing large diametral expansion. Fig. 9 shows the pressure–diameter response of the balloon with material parameters given in Table 5.

Due to the symmetry of the problem, only a quarter of the geometry has been considered (see Fig. 10). The total load in the model has been applied in three steps: (i) the residual stress is imposed in the model through an initial deformation gradient, as proposed by Rodriguez et al. (1994); (ii) the artery is inflated up to a pressure of 13.3 kPa (100 mmHg), assumed to be the mean arterial pressure (physiological conditions); (iii) the balloon is inflated up to a pressure of 200 kPa (2 bar). The internal surface of the artery and the external surface of the balloon where used to define a frictionless contact pair to model the inflation process in the last step.

Fig. 10 shows the undeformed and deformed configurations of the artery upon balloon inflation. Note that this loading causes a considerable amount of circumferential and longitudinal stretching in the artery in the area around the balloon end. This particular deformation will cause a larger stretching in the fibers oriented at wider angles with respect the circumferential direction, than for those closely packed along the circumferential direction of the artery.

Fig. 11 shows the damage distribution in the arterial wall after balloon inflation for the two models. Both models predict damage to occur at the adventitia layer where fibers are oriented at 40° with respect to the circumferential direction and, therefore, being subjected to a larger stretch as mentioned before. In fact, the fiber stretch in the zone of maximum damage is around 1.05 which corresponds to a damage value of 0.21 according to (51) and the parameters given in Table 4. However, the amount and distribution of damage in both models is quite different. While for the stochastic model damage is distributed more uniformly along the artery, where fibers experience larger stretching (as expected for a strain-driven model), for the continuum model, damage is highly localized near the balloon end. Even though the location of damage near the balloon end is expected and also observed by other authors (Gasser and Holzapfel, 2006), the fact that damage appears in the adventitia layer might result surprising since damage is expected in the media. However, the results obtained by

Table 4
Model parameters used for the computations of the balloon inflation of the coronary artery

	C_1 (kPa)	D_1 (kPa)	γ	η	κ	δ	θ	ϕ
Media	27.4	0.425	23.7	1.1	1.9	1.949	18.9	10°
Adventitia	2.7	0.4	21.7	1.25	1.57	1.949	18.9	40°

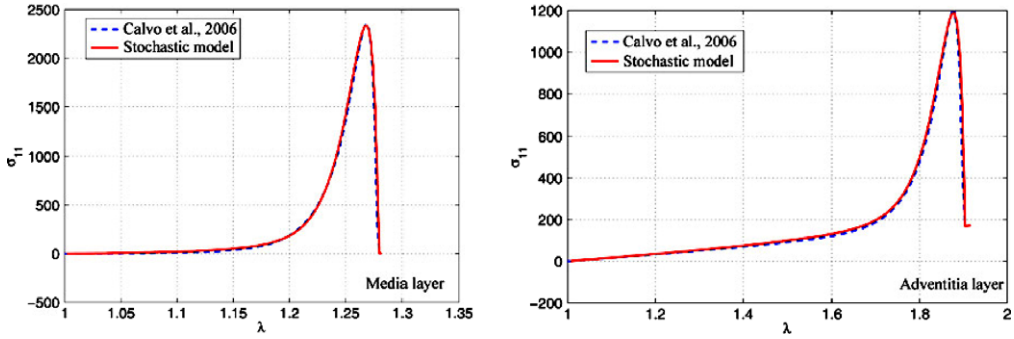

Fig. 8. Uniaxial stress–stretch response for both models showing the excellent agreement between them for the primary loading path.

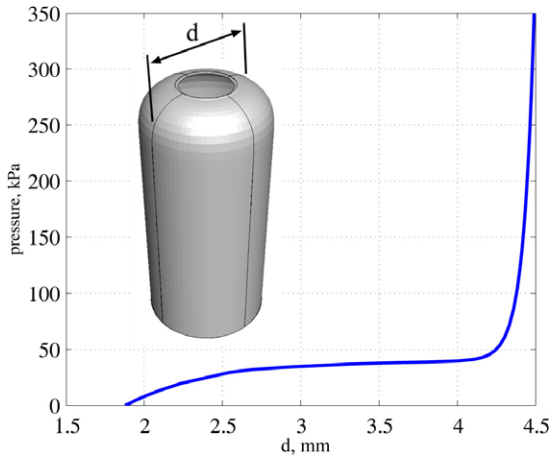

Fig. 9. Pressure–diameter curve for the Grüntzig-type balloon used in the simulations.

Table 5
Material parameters used in the material model of the balloon according to Gasser and Holzapfel (2006)

c (MPa)	k_{1l} (MPa)	k_{2l}	k_{1c} (MPa)	k_{2c}
0.5	500.0	0.01	0.001	0.55

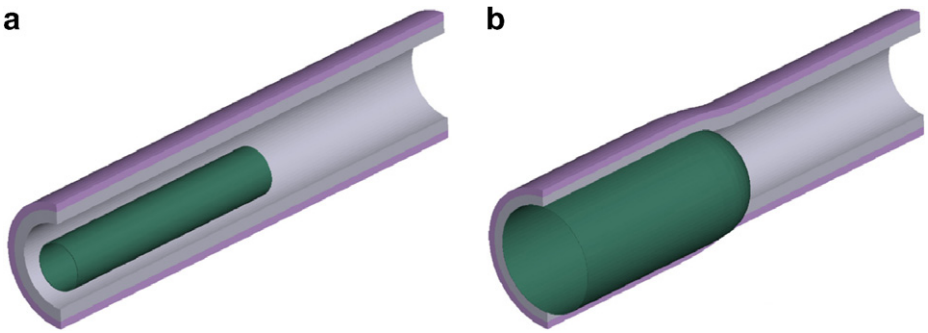

Fig. 10. Artery and balloon geometries: (a) initial unloaded configuration; (b) deformed configuration upon balloon inflation at 2 bar, the artery has been previously subjected to physiological pressure and initial stress.

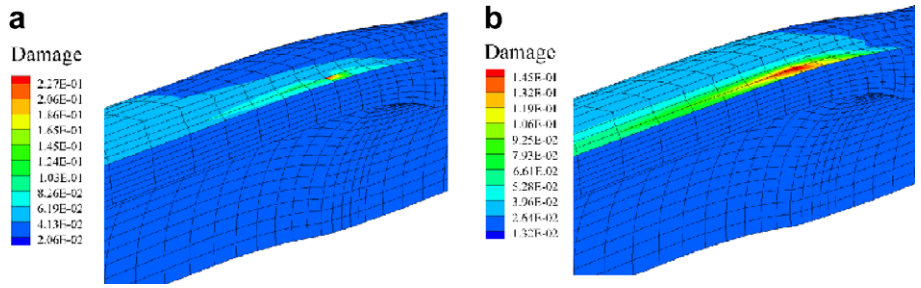

Fig. 11. Distribution of damage in the artery after balloon inflation: (a) continuum model; (b) stochastic model.

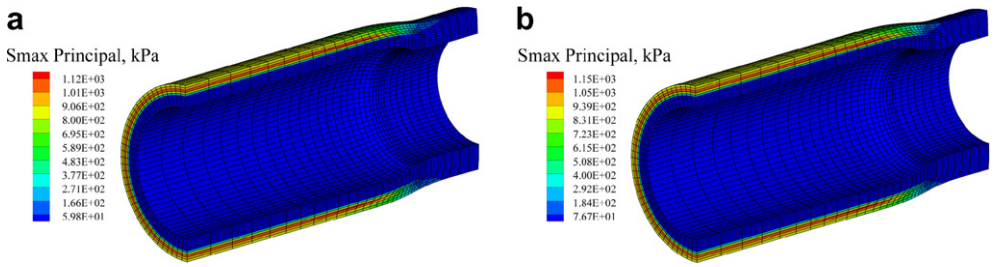

Fig. 12. Maximum principal Cauchy stress in the arterial wall for both models after balloon inflation: (a) continuum model; (b) stochastic model.

Gasser and Holzapfel (2006) show a remarkable larger stress in the adventitia layer (about four times larger) than in the media, as also obtained in the present simulation (see below). For this particular stress field, and for the damage models here considered, more damage should develop in the adventitia layer. This results could be due to a number of reasons like an improper setting of the residual stress state in the load free configuration, or bad specification of material constants and structural parameters of the model. However, we have used numerical values reported in the literature and the results here obtained coincide with those reported by others for similar problems.

Fig. 12 depicts the Cauchy stress distribution in the artery for both models. Note that even though the stress magnitude is similar for both models, the stress distribution is more uniform along the artery for the stochastic than for the continuum model. In fact, the area of maximum stress localization for the continuum model coincides with the zone where maximum damage occurs, while for the stochastic model, the damage affects a wider area. These results might be related to the damage criterion in both models. For the continuum model damage criterion is based on energy while for the continuum model it is based on fiber stretch. This might make the continuum damage model more sensitive to stress gradients than the stochastic one as observed in this example.

6. Conclusions

3D anisotropic constitutive damage models at finite strains for fibrous soft biological tissues have been described and compared. Decoupled damage mechanisms for the matrix and fibers are considered in both models, and characterized by the maximum value previously attained by the strain–energy of the undamaged material. For the fibrous part, the continuum model proposes a similar mechanism as for the matrix, while the stochastic model assumes a different strain–energy to failure for each fibril within the fiber bundle, with the distribution following a Beta probability density function.

Both models have been implemented in the Finite Element framework under large deformations, and closed form expressions of the decoupled tangent elasticity tensors are given in the paper. Numerical examples under finite strains show a similar performance for both models. In all examples, the continuum model showed larger localization of damage than the stochastic one, with damage being localized near zones of large stress gradi-

ents. In the uniaxial test, we observed that for a given stretch for which the stochastic model has lower damage than the continuum one, the rate of stress lowering after unloading was always larger in the stochastic model than in the continuum model (see Figs. 2 and 3). This characteristic is associated with the fact that the model assumes fiber bundles as composed of fibrils with different strain to failure in which shorter fibrils fail first. Therefore, recruitment of the remaining fibers will occur at larger stretch values with a rapid stiffening as fibrils approach their full extended length. In addition, damage for the stochastic model was always located in areas of large fiber stretch (as expected in a strain-driven damage model).

Acknowledgments

The authors gratefully acknowledge research support from the Spanish Ministry of Science and Technology through the research projects DPI2004-07410-C03-01, and FIS2005-05020-C03-03, and the Sixth Framework Programme through the project FP6-2002-SME-1-513226.

References

Alastrué, V., Calvo, B., Peña, E., Doblare, M., 2006. Biomechanical modelling of refractive corneal surgery. ASME J. Biomech. Eng., 128.

Arnoux, P.J., Chabrand, P., Jean, M., Bonnoit, J., 2002. A visco-hyperelastic with damage for the knee ligaments under dynamic constraints. Comp. Methods Biomech. Biomed. Eng. 5, 167–174.

Arruda, E.M., Boyce, M.C., 1993. A three-dimensional constitutive model for the large stretch behavior of rubber elastic materials. J. Mech. Phys. Solids 41, 389–412.

Balzani, D., Schröder, J., Gross, D., 2006. Simulation of discontinuous damage incorporating residual stress in circumferentially overstretched atherosclerotic arteries. Acta Biomater. 2, 609–618.

Billiar, K.L., Sacks, M.S., 2000. Biaxial mechanical properties of fresh and glutaraldehyde treated porcine aortic valve cusps. Part ii: a structurally guided constitutive model. ASME J. Biomech. Eng. 122, 327–335.

Calvo, B., Peña, E., Martinez, M.A., Doblaré, M., 2006. An uncoupled directional damage model for fibred biological soft tissues, formulation and computational aspects. Int. J. Numer. Methods Eng. 06, 1–30.

Canham, P.B., Finlay, H.M., Boughner, D.R., 1997. Contrasting structure of the saphenous vein and internal mammary artery used as coronary bypass vessels. Cardiovasc. Res. 34, 557–567.

Chew, P.H., Yin, F.C., Zeger, S.L., 1986. Biaxial stress–strain properties of canine pericardium. J. Mol. Cell Cardiol. 18, 567–578.

Decraemer, W.F., Maes, M., Vanhuyse, V.J., 1980. An elastic stress–strain relation for soft biological tissues based on a structural model. J. Biomech. 13, 463–468.

Dingemans, K.P., Teeling, P., Lagendijk, J.H., Becker, A.E., 2000. Extracellular matrix of the human aortic media: an ultrastructural histochemical and immunohistochemical study of the adult aortic media. Anat. Rec. 258, 1–14.

Farquhar, T., Dawson, P.R., Torzilli, P.A., 1990. A microstructural model for the anisotropic drained stiffness of articular cartilage. ASME J. Biomech. Eng. 112, 414–425.

Flory, P.J., 1961. Thermodynamic relations for high elastic materials. T Faraday Soc. 57, 829–838.

Fung, Y.C., 1993. Biomechanics: Mechanical Properties of Living Tissues. Springer-Verlag, Berlin.

Gasser, T.C., Holzapfel, G.A., 2002. A rate-independent elastoplastic constitutive model for (biological) fiber-reinforced composites at finite strains: continuum basis, algorithmic and finite element implementation. Comput. Mech. 29, 340–360.

Gasser, T.C., Holzapfel, G.A., 2006. Finite element modeling of balloon angioplasty by considering overstretch of remnant non-diseased tissues in lesions. Comput. Mech.

Gasser, T.C., Ogden, R.W., Holzapfel, G.A., 2006. Hyperelastic modelling of arterial layers with distributed collagen fibre orientations. J. R Soc. Interface 3, 15–35.

Gasser, T.C., Schulze-Bauer, C.A.J., Holzapfel, G.A., 2002. A three-dimensional finite element model for arterial clamping. ASME J. Biomech. Eng. 124, 355–363.

Hokanson, J., Yazdami, S., 1997. A constitutive model of the artery with damage. Mech. Res. Commun. 24, 151–159.

Holzapfel, G.A., 2000. Nonlinear Solid Mechanics. Wiley, New York.

Holzapfel, G.A., Gasser, T.C., Ogden, R., 2000. A new constitutive framework for arterial wall mechanics and a comparative study of material models. J. Elasticity 61, 1–48.

Holzapfel, G.A., Stadler, M., Schulze-Bauer, C.A.J., 2002. A layer specific three-dimensional model for the simulation of balloon angioplasty using magnetic resonance imaging and mechanical testing. Ann. Biomed. Eng. 30, 753–767.

Holzapfel, G.A., Weizsäcker, H.W., 1998. Biomechanical behavior of the arterial wall and its numerical characterization. Comput. Biol. Med. 28, 377–392.

Holzapfel, G.A., Ogden, R.W. (Eds.), 2006. Mechanics of Biological Tissue. Springer-Verlag, Heidelberg.

Hsu, E.W., Muzikant, A.L., Matulevicius, S.A., Penland, R.C., Henriquez, C.S., 1998. Magnetic resonance myocardial fiber-orientation mapping with direct histological correlation. Am. J. Physiol. Heart Circ. Physiol. 274, 1627–1634.

Humphrey, J.D., 2002. Cardiovascular Solid Mechanics. Springer, New York.

Hurschler, C., Loitz-Ramage, B., Vanderby, R., 1997. A structurally based stress–stretch relationship for tendon and ligament. J. Biomech. Eng. 119, 392–399.

Lanir, Y., 1983. Constitutive equations for fibrous connective tissues. J. Biomech. 16, 1–12.

Marsden, J.E., Hughes, T.J.R., 1994. Mathematical Foundations of Elasticity. Dover, NY.

Naghdi, P.M., Trapp, J.A., 1975. The significance of formulating plasticity theory with reference to loading surfaces in strain space. Int. J. Eng. Sci. 13, 785–797.

Natali, A.N., Pavan, P.G., Carniel, E.L., Luisiano, M.E., Taglialavoro, G., 2005. Anisotropic elasto-damage constitutive model for the biomechanical analysis of tendons. Med. Eng. Phys. 27, 209–214.

Neto, E.A.S., Peric, D., Owen, D.R.J., 1998. Continuum modelling and numerical simulation of material damage at finite strains. Arch. Comput. Method Eng. 5, 311–384.

Ogden, R.W., 1978. Nearly isochoric elastic deformations: application to rubberlike solids. J. Mech. Phys. Solids 26, 37–57.

Oktay, H.S., 1993. Continuum damage mechanics of ballon angioplasty. Internal Report, UMI.

Peña, E., Calvo, B., Martinez, M.A., Doblaré, M., 2005. A three-dimensional finite element analysis of the combined behavior of ligaments and menisci in the healthy human knee joint. J. Biomech. 39, 1686–1701.

Pioletti, D.P., Rakotomanana, L., 2000. Finite element model of the anterior cruciate ligament. Eur. J. Mech. A/Solids 19, 749–759.

Rodríguez, J.F., Cacho, F., Bea, J.A., Doblaré, M., 2006. A stochastic-structurally based three-dimensional finite-strain damage model for fibrous soft tissue. J. Mech. Phys. Sol. 54, 564–886.

Rodriguez, E.K., Hoger, A., McCulloch, A., 1994. Stress-dependent finite growth in soft elastic tissues. J. Biomech. 27, 455–467.

Sacks, M.S., 2000. Biaxial mechanical evaluation of planar biological materials. J. Elasticity 61, 199–246.

Sacks, M.S., 2003. Incorporation of experimentally-derived fiber orientation into a structural constitutive model for planar collagenous tissues. ASME J. Biomech. Eng. 125, 280–287.

Sacks, M.S., Chuong, C.J., More, R., 1994. Collagen fiber architecture of bovine pericardium. ASAIO J. 40, 632–637.

Samila, Z.J., Carter, S.A., 1981. The effect of age on the unfolding of elastin lamellae and collagen fibers with stretch in human carotid arteries. Can. J. Physiol. Pharmacol. 59, 1050–1057.

Schechtman, H., Bader, D.L., 2002. Fatigue damage of human tendons. J. Biomech. 35, 347–353.

Simo, J.C., 1987. On a fully three-dimensional finite-strain viscoelastic damage model: formulation and computational aspects. Comput. Methods Appl. Mech. Eng. 60, 153–173.

Simo, J.C., Hughes, T., 1998. Computational Inelasticity. Springer-Verlag, New York.

Simo, J.C., Ju, J.W., 1987a. Strain- and stress-based continuum damage models. I: formulation. Int. J. Solids Struct. 23, 821–840.

Simo, J.C., Ju, J.W., 1987b. Strain- and stress-based continuum damage models. II: computational aspects. Int. J. Solids Struct. 23, 841–870.

Simo, J.C., Taylor, R.L., 1985. Consistent tangent operators for rate-independent elastoplasticity. Comput. Methods Appl. Mech. Eng. 48, 101–118.

Spencer, A.J.M., 1954. Theory of invarinats. Continuum Physics. Academic Press, New York, pp. 239–253.

Weiss, J., 1994. A constitutive model and finite element representation for transversely isotropic soft tissues. Ph.D. thesis, The University of Utah.

Weiss, J., Maker, B., Govindjee, S., 1996. Finite element implementation of incompressible, transversely isotropic hyperelasticity. Comput. Methods Appl. Mech. Eng. 135, 107–128.

Wuyts, F.L., Vanhuyse, V.J., Langewouters, G.J., Decraemer, W.F., Raman, E.R., Buyle, S., 1995. Elastic properties of human aortas in relation to age and atherosclerosis: a structural model. Phys. Med. Biol. 40, 1577–1597.

Zulliger, M.A., Fridez, K.H.P., Stergiopulos, N., 2004. A strain energy function for arteries accounting for wall composition and structure. J. Biomech. 37, 989–1000.